

Impinging jet cleaning of tank walls: effect of jet length, wall curvature and related phenomena

Chee, M.W.L, Ahuja, T.V, Bhagat, R.K, Taesopapong, N, Wan, S.A, Wigmore, R.L, and Wilson, D.I.
Department of Chemical Engineering and Biotechnology, Philippa Fawcett Drive, Cambridge,
CB3 0AS, UK

Revised Manuscript FBP 2018 323

Submitted to

Food & Bioproducts Processing

2018

Corresponding author

D. Ian Wilson

Department of Chemical Engineering and Biotechnology

Philippa Fawcett Drive

Cambridge

CB3 0AS

UK

Tel +44 1223 334 791

E-mail diw11@cam.ac.uk

Impinging jet cleaning of tank walls: effect of jet length, wall curvature and related phenomena

Chee, M.W.L, Ahuja, T.V, Bhagat, R.K, Taesopapong, N, Wan, S.A, Wigmore, R.L, and Wilson, D.I.
Department of Chemical Engineering and Biotechnology, Philippa Fawcett Drive, Cambridge,
CB3 0AS, UK

Abstract

The effect of jet length and wall curvature on the flow patterns generated by an impinging water jet were quantified and the effect on cleaning investigated in a brief study. The length of time taken to establish steady flow was characterised. Jet impingement on a flat vertical wall was investigated for jets of diameter 2 – 4 mm for lengths, L , up to 1 m. The amount of liquid lost to splatter was measured and found to be insensitive to L for short L (< 300 mm for these nozzles) and strongly related to L for longer values. The shape of the radial flow zone on flat walls agreed with existing models once the fraction of liquid lost to splatter was accounted for. Tests on horizontal and vertical cylinders with curvatures in the range 6.9 to 20 m⁻¹ showed that the curvature of the impinged wall did not affect the shape of the radial flow zone until higher flow rates (> 1.5 dm³ min⁻¹). The cleaning of two viscoplastic model food soils was studied briefly: a hydrophobic petroleum jelly and Carbopol[®], a water-soluble gel. The splatter correction was not able to account for all the differences observed in cleaning at different jet lengths. There was no appreciable effect of curvature on cleaning behaviour. Soaking of the Carbopol[®] increased its cleaning rate.

Keywords Breakup, cleaning, curvature, hydrodynamics, hydraulic jump, jet.

Introduction

Liquid jets generated by rotating nozzles or spray balls are regularly employed as components of cleaning-in-place (CIP) systems and are used to distribute cleaning solutions and rinsing liquid around the walls of tanks, reactors and other process vessels. Quantitative models of the hydrodynamics of the flow generated by a coherent liquid jet impinging on a flat vertical wall have been developed in the last decade and combined with cleaning models to predict the removal of soil layers from such walls (*e.g.* Glover *et al.*, 2016; Bhagat *et al.*, 2017). After impingement, the liquid, which in the food sector is usually water or a solution thereof, spreads radially outwards in a thin, fast moving film until surface tension causes a transition to a slower moving, thicker film region. With a vertical wall, an almost circular jump forms initially. Above the point of impingement this gives rise to a film jump with a narrow band (or rope) of liquid which flows circumferentially downwards beyond it. Below the point of impingement, gravity causes this initial jump to evolve into a draining film, bounded by the ropes which join from above and form the boundaries of the falling film (Aouad *et al.*, 2016; Bhagat *et al.*, 2018).

Impinging jets therefore generate two regions of flow which can promote cleaning. In the area within the jump, here termed the radial flow zone (RFZ), the thin film of liquid is fast moving and exerts a high shear stress, which can promote cleaning. In the falling film the shear stresses are smaller but the area is considerably larger, achieving contact of the soil with the cleaning solution and promoting any weakening of the deposit associated with soaking. The wall shear stress exerted in the rope region is intermediate between the other two regions.

Wilson *et al.* (2012) modelled the flow in the RFZ as a laminar film with a parabolic velocity profile similar to that in Nusselt's analysis of film condensation (Nusselt, 1916). The location of the film jump was obtained from a balance between the outward flow of momentum in the liquid and the surface tension force opposing wetting, giving

$$R = 0.276 \left[\frac{\rho^2 Q^3}{\mu \gamma (1 - \cos \beta)} \right]^{1/4} \quad [1]$$

where R is the half-width of the RFZ at the level of the point of impingement, ρ the liquid density, Q the volumetric flow rate through the nozzle, μ the liquid dynamic viscosity, γ the vapour-liquid surface tension and β the solid-liquid contact angle. The model includes a

contribution from the wall material via β . A more rigorous treatment of the flow in the RFZ and formation of the film jump was given by Bhagat and Wilson (2016). Equation [1] provides a reasonable first order estimate of R .

Much of the work on impinging jet hydrodynamics (*e.g.* Watson, 1964; Bush and Aristoff, 2003; Wilson *et al.*, 2012; Aouad *et al.*, 2016) has employed coherent jets impinging normally on flat walls. The jets employed in practice are subject to several phenomena which affect the transfer of those results to industrial systems. Figure 1 presents some of the considerations that need to be considered in scaling up the results to industrial scales. Spray balls and CIP nozzles do not normally generate coherent jets and the jet is often subject to breakup, which is promoted by the length that the jet has to travel from the nozzle before striking the wall. Nozzle motion (usually rotation) and gravity mean that the jet will rarely impinge normally on a wall. The effect of oblique impingement by coherent jets was considered by Bhagat *et al.* (2017). The other factors have not received much attention to date.

The effect of jet length, L , was investigated by Feldung Damkjær *et al.* (2017), who reported a scale up study employing industrial nozzles in a full size tank with nozzle diameters, d_N , ranging from 2.0 to 5.5 mm and nozzle volumetric flow rates, ($Q = 0.8 - 50 \text{ dm}^3 \text{ min}^{-1}$; $0.05 - 30 \text{ m}^3 \text{ h}^{-1}$) representative of industrial installations. They considered jet lengths of 80 – 2490 mm impinging normally on a flat, transparent, vertical target plate and found that the hydrodynamic and cleaning behaviour was reasonably well described by the existing models (*e.g.* Wilson *et al.*, 2012) for the 2 mm nozzles at low L ($< 200 \text{ mm}$). They attributed the observed differences at higher L to the combined effects of jet breakup, wherein the liquid forms a procession of droplets, and splatter, whereby a fraction of the liquid rebounds from the wall and does not join the spreading film. They showed that the dimensions of the film jumps (*i.e.* height *vs.* width) agreed with the predictions of the Bhagat and Wilson (2016) model. They concluded that existing models for the RFZ could be used if the flow rate used in the expressions was corrected for losses due to splatter.

They also studied the rate of cleaning of petroleum jelly layers and found that longer jets often gave cleaning behaviour which differed from that observed with a coherent jet. A jet impinging normally on a wall creates a circular region within the RFZ which grows with time: Feldung Damkjær *et al.* fitted their measurements to the cleaning model of Glover *et al.* (2016) and

reported that the cleaning rate constant extracted from tests with longer jets was smaller than that **expected from tests** with coherent jet tests. **The** difference could not be explained simply in terms of adjusting the flow rate. These observations indicate that the dynamics associated with jet breakup and drop impact need to be considered in scale-up studies.

Phenomena related to splatter caused by jets impinging on flat walls has been studied for well-defined coherent jets by Errico (1986), Lienhard *et al.* (1992) and Bhunia and Lienhard (1994). Liquid can be lost from the main flow by rebound or shedding from film boundaries. The mechanics of jet breakup and splatter are complex (see review by Eggers and Villermaux, 2008) even for well-defined jets generated in carefully designed nozzles. Nozzles used in industrial practice are not usually designed to deliver coherent jets and an effective method of characterising these flows is therefore required.

Wang *et al.* (2013) quantified the effect of splatter from short ($L = 50$ mm) jets generated by 2, 3 and 4 mm diameter convergent nozzles impinging on vertical walls using an apparatus similar to that used in this work. They reported their results in terms of the splatter fraction, S , defined as

$$Q_{\text{eff}} = Q(1 - S) \quad [2]$$

where Q_{eff} is the volumetric flow rate in the falling film. They found that S was small until the jet Reynolds number (defined $Re = U_o d_N / \nu$, where U_o is the **jet velocity** and ν the **liquid** kinematic viscosity) exceeded 12 000. Above this value S increased linearly with Re reaching $S = 0.37$ at $Re = 20\,000$. The value of S also depended on the angle of impingement (see Wang *et al.*, 2013). **Feldung Damkjær *et al.* reported Q_{eff}/Q data corresponding to S values, calculated using $S = 1 - Q/Q_{\text{eff}}$, up to 0.7. They estimated Q_{eff} by using Equation [1] to determine the flow rate which would have given the observed value of R .**

This paper reports an experimental investigation of a subset of the factors identified in Figure 1 on impinging jet behaviour. The effect of jet length and breakup on the shape of the RFZ and splatter is considered for longer jet lengths (up to 1 m) than the study of Wang *et al.* The effect of jet length on cleaning is investigated briefly via testing on a hydrophobic soil, petroleum jelly, similar to those employed by Feldung Damkjær *et al.* and Glover *et al.*

A second aspect which has received little attention is the curvature of the wall. As a first step towards understanding these effects, the effect of jet length and wall curvature on jet hydrodynamics was investigated for vertical and horizontal cylinders. Whilst wall curvature is not expected to be large for tanks (as curvature is related to radius^{-1} , and the liquid film thickness is submillimetre), it could be important for smaller items (bottles, small fermenters).

The third aspect, which is considered briefly, is the effect of soil contact with the liquid before being exposed to the jet, *i.e.* soaking. This will occur in practice when a soil is contacted by liquid draining from above. Many food soils weaken on soaking. Layers of Carbopol[®] gel were used for these tests. Carbopol[®] gels are suspensions of crosslinked polyacrylic acid polymer in water and are often used as model viscoplastic fluids (Dinkgreve *et al.*, 2018). Their yield stress depends on the volume fraction of polymer and pH, so extended contact with water is expected to reduce the yield stress and promote liquid-like behaviour.

Materials and Methods

Tests were conducted with tap water at room temperature using the apparatus and brass convergent nozzles with diameter, d_N , of 2, 3 and 4 mm employed by Wang *et al.* (2013). Water was pumped from a tank through a rotameter and flow control valves before entering a 7.5 mm i.d. steel pipe which served as a flow straightening section ahead of the nozzle. Pipe lengths of 150 mm and 350 mm were used. The volumetric flow rate through the nozzle, Q , was read from the rotameter which had been calibrated separately.

Horizontal jets were used in the majority of tests. The nozzle was located at horizontal distance L from the target. At lower flow rates, jet droop could be significant and in some cases the jet did not reach the target: for others the inclination of the nozzle was adjusted to ensure that the jet impinged horizontally. Photographs of the jet from the side indicated that the midpoint of the jet followed the trajectory expected from gravity, namely $z = -gx^2/2U_o^2$, where g is the acceleration due to gravity, x the horizontal distance travelled by the jet and z the vertical displacement.

All targets used were transparent. Photographs and videos of the flow pattern at and near the point of impingement were taken from the dry side of the transparent target with a Nikon D3300 or Sony Cyber-shot RX100V digital camera, aligned co-axial with the jet. Transparent graticule

tape was placed on the dry side of the target to provide a length calibration for image processing.

Flow patterns

Figure 2(a) shows the dimensions of the flow pattern extracted from photographs: the half-width of the RFZ at the level of the point of impingement, R , and the half-width of the wetted region, R_c ; and the height of the jump and the top of the rope, Z and Z_c , respectively. The photograph shows a case where the flow pattern was not symmetrical about the vertical midplane, which is captured in the large error bars used in reporting R and R_c .

The evolution of these parameters over time, t , for a jet impinging on an initially dry target is illustrated in Figure 2(b). It can be seen that R and Z were initially almost equal, with Z slightly smaller due to gravity. After 0.1 s the rapid growth stops and R and Z differ (one increases, the other decreases) as the rope is established over the next 0.2 s. R_c stabilised after a further 0.2 s, 0.5 s after the initial impact. A detailed account of the formation of the initial film jump is given in Bhagat *et al.* (2018): the change in R and Z in the period $0.1 \text{ s} < t < 0.3 \text{ s}$ are associated with establishment of the boundary conditions downstream, *i.e.* as the rope develops. At the top of the RFZ, the rope flows over the top of the thin film. Regular fluctuations are evident thereafter in Z , indicating that the flow at the top of the rope was unstable. The time taken to establish the radial flow zone, t_E , was measured for a 2.67 mm nozzle at a number of flow rates using a high speed camera (Photron FASTCAM SA3).

Jet length and splatter

To investigate the effect of jet length, a $360 \times 600 \times 5 \text{ mm}$ (width \times height \times depth) flat vertical Perspex[®] (polymethylmethacrylate, PMMA) wall was used as the target. The jet lengths and flow rates tested for each nozzle, and the associated jet velocities, Reynolds and Weber ($We = \rho U_o^2 d_N / \gamma$) numbers are summarised in Table 1.

The volumetric flow rate in the falling film, Q_{eff} , was measured by collecting the water in a wide reservoir located at the base of the target. The reservoir was fitted with a slotted roof so that droplets originating from the jet due to breakup or droplets from rebound off the target were unlikely to be collected.

Wall curvature

The effect of wall curvature on the flow pattern was investigated by impinging the jet on the inner wall of a Perspex[®] cylinder. Four cylinders were tested with inner diameter, D , ranging from 10 to 29 cm and wall curvature, $\kappa = 2/D$, from 20 to 6.9 m⁻¹ (see Table 2). The flat wall served as a control with $\kappa = 0$. The feed pipe passed through a 40 × 40 mm slot in the cylinder wall and the $d_N = 2$ mm nozzle was used to generate a coherent jet impinging normally on the inner wall (with $L = 30$ mm). The target cylinder was mounted with its axis vertical or horizontal. A photograph of a horizontal cylinder experiment is given in Figure 7(a). The experimental conditions are summarised in Table 3.

The dimensions labelled in Figure 2(a) were calculated from photographs taken by the main camera located externally, again aligned co-axial with the jet. The dimensions extracted from the images were corrected for refraction effects which did not arise with flat walls. Appendix A describes the approach taken: the estimates were compared with measurements made by a second camera which was moved around the apparatus in order to obtain refraction-free images.

Cleaning

Short sets of cleaning experiments were performed on walls coated with thin layers of petroleum jelly (APC Pure, UK), a hydrophobic yield stress fluid, or ClearglideTM, a commercial viscoplastic suspension of Carbopol[®] (crosslinked polyacrylic acid polymer) in water. The static yield stress of the petroleum jelly, measured using a Kinexus Lab+ Rheometer (Malvern Instruments, UK), was approximately 220 Pa (R.R. Fernandes, internal communication). The yield stress of the Carbopol[®], measured using a vane tool, decreased from approximately 20 Pa to 5 Pa when diluted 1:1 with water (D. Gibson, internal communication). Layers of the required thickness were prepared on an initially dry target using the spreading tool described by Glover *et al.* (2016). Petroleum jelly layers were rested for 30 minutes before cleaning while Carbopol[®] layers were cleaned immediately after preparation. The targets were mounted vertically and subjected to jet impingement while being videod. A dark food grade dye was added to the Carbopol[®] gel to make it easier to determine when material had been removed from the wall. With both materials the cleaned area took the form of a circle centred on the point of impingement which grew over time. The radius of the circle, a , was extracted from images using a MATLAB script.

Results and Discussion

Formation of steady flow patterns

These tests were conducted with steady flows, which are directly related to continuous jets generated by static and moving nozzles. Other workers (*e.g.* Fuchs *et al.*, 2017) have investigated the use of intermittent jets as a means of increasing efficiencies based on total water consumption. In these, a steady flow is applied for a period t_B , followed by a period where no jet impacts and the liquid drains away (if the wall is inclined). The time taken to establish the radial flow zone, labelled t_E (between 0.1 and 0.2 s in Figure 2(b)) is an important parameter in such applications as it constitutes a characteristic timescale for the periodicity of bursts: a shorter t_B would result in the liquid establishing a smaller RFZ (the region of mechanically assisted cleaning), while longer periods would only influence the width of the wetted region below the point of impingement. A short series of tests were conducted to establish this timescale. This discussion focuses on RFZ formation, as the dynamics of the wetted region were not explored in the experiments.

The measured values of t_E can be compared with an estimate based on the Wilson *et al.* (2012) model, detailed in Appendix B,

$$t_E = 0.0477 \frac{\rho Q}{\gamma(1 - \cos \beta)} \quad [3]$$

Figure 3 shows that Equation [3] gives a reasonable estimate of the magnitude of t_E but does not capture the dependency on jet diameter, or jet velocity for a given flow rate. Also shown in the Figure are the predictions for t_E obtained with the more detailed model for the flow in the thin film by Bhagat and Wilson (2016). This gives a more accurate description of the effect of flow rate for the limited number of experimental results presented.

Effect of jet length

The shortest ($L \leq 70$ mm) jets were coherent. Surface fluctuations were evident on all longer jets, and breakup was observed at lower Reynolds numbers with $L \geq 350$ mm. The splatter fraction data in Figure 4 show a transition in splatter behaviour with increasing L , but this is not associated with a transition to jet breakup. For the flow rates and nozzle sizes studied, the Reynolds and Weber numbers indicate that jet breakup is associated with the first wind-assisted

regime (see Lin and Reitz, 1998). However, the applicability of correlations obtained for well-defined jets (long cylindrical nozzles, *etc.*) to the nozzles employed here (short, convergent entry angle of $55^\circ \pm 10^\circ$) is expected to be limited.

For shorter jets, $L < 300$ mm, the data exhibit an almost linear increase in S for $Re > 13\,000$, which is consistent with the behaviour reported by Wang *et al.* (2013). The trend is almost independent of d_N , indicating that the Reynolds number captures the effect of jet diameter in this regime.

For longer jets, $L > 300$ mm, there is a noticeable transition to S being independent of Re and strongly dependent on L , with a weak dependence on d_N (see Figure 4(b)). S approaches 0.4 for the longest jets, indicating that a significant fraction of the liquid delivered by the nozzle does not appear in the draining film. It was not possible using this apparatus to differentiate between water lost as a result of jet breakup and that lost from rebound. The interplay of d_N and L extends until $L > 0.5$ m: plotting the data in Figure 4(b) against L/d_N did not yield further insight (see Supplementary Figure S1). For $L = 1$ m, S is almost insensitive to Re , d_N and Q , so there is no advantage to using a particular nozzle to deliver a given flow rate of water in the jet (but this will affect the pressure drop in the line).

Splatter was not determined solely by jet breakup: for the longer jets, the value of S did not change appreciably when the jet was breaking up into droplets (indicated by open symbols in the Figure). Splatter is attributed to the momentum of the drops formed as the jet breaks up and whether this is large enough for rebound to occur. It is also related to the stability of the film and rope, and whether surface tension is strong enough to prevent these shedding droplets.

Similar trends were reported for industrial scale nozzles by Feldung Damkjær *et al.* (2017). Their Q_{eff}/Q data are reported as S against Re in Supplementary Figure S2. In their case, jets with $L \leq 300$ mm exhibited the trend of increasing S with Re which is not evident for longer jets. The values of S are noticeably larger than the current work. It should be noted that Q_{eff} in these tests was estimated from Equation [1].

The radial flow zone dimensions, R and Z , increased with flow rate. Figure 5 shows that these collapsed to common trends when R is plotted against Q_{eff} , indicating that the splatter fraction correction is partly able to account for the differences in fluid flow behaviour. There is still

some variation, however, and this is evident when the data are compared with the Wilson *et al.* (2012) model (Equation [1]) with $\beta = \pi/2$.

The shape of the radial flow zone (see inset in Figure 5) follows the same trend for all cases, with $Z \approx 4R/5$, indicating the influence of gravity on the steady state RFZ shape. The common trend suggests that there is no change in flow regime over the range of flow rates studied. Figure 5 supports the findings of Feldung Damkjær *et al.*, who estimated the splatter fraction in their experiments.

The width of the draining film is related to R_c , this being the half-width of the wetted region at the level of the point of impingement. The data fitted the relationship $R_c = 4R/3$ reported by Wang *et al.* (2013) well (Supplementary Figure S3).

Effect of wall curvature

The flow patterns generated by the impinging water jet on cylindrical target walls were similar to those observed with flat walls, namely radial flow near the impingement point, a film jump above this point, and a confining rope of falling liquid.

Figure 6 summarises the effect of wall curvature on the dimensions of the radial flow zone, Z and R , at different flow rates ($4\,200 < Re < 21\,000$). For vertical cylinders, the height of the film jump, Z , does not change appreciably with curvature at lower flow rates. This might be expected since the flow in the Z direction is not subject to curvature. As the flow rate increases, the variation that occurs is attributed to splatter as there was noticeable spray observed within the cylinders. The half-width of the radial flow zone, R , is similarly insensitive to curvature (within experimental error) at lower flow rates. At higher flow rates, there is a steady decrease in R with increasing curvature. In vertical cylinders, the flow in the azimuthal direction is subject to curvature effects, so the results suggest that the amount of splatter increases (so Q_{eff} , decreases and thus R decreases) as κ increases.

Horizontal cylinders were expected to show the opposite behaviour, but little variation was observed at lower flow rates while a decrease with κ was observed at higher flow rates for both Z and R . The decrease at higher flow rates is attributed to splatter. The spray observed within the cylinders was noticeably stronger with horizontal cylinders than vertical cylinders,

demonstrating the complexity of these wall curvature effects. Quantitative measurements of splatter could not be made in the cylinder tests due to the limitations of the experimental set up.

These results demonstrate that a positive curvature of the wall, as arises with jets striking the internal wall of a cylinder, has a slight effect on the behaviour of the radial film pattern. The width of the rope, B , did not change appreciably as a result of wall curvature (see Supplementary Figure S4).

The curvatures studied here are larger than those likely to be encountered in tanks for food manufacturing applications, so the influence of curvature in practice is therefore expected to be small. Splatter measurements were not made in the cylinder tests. Furthermore, the results presented here have been collected for concave walls: the impact of a convex wall on splatter has not been studied and represents an avenue for further work as these are often encountered in CIP applications as piping, fitting connections and other protuberances.

Larger jet diameters and higher flow rates were also investigated. At higher flow rates the radial flow zone extended further around the cylinder inner wall. Two flow patterns not seen on flat walls were observed in experiments with horizontal cylinders: shedding (Figure 7(a)) and wraparound (Figure 7(b)).

Figure 7(a) shows an example in a horizontal cylinder where gravity causes water to be shed from the rope above the nozzle. Shedding is not expected to affect the liquid velocity in the RFZ, but it will reduce the flow rate in the rope.

At sufficiently high flow rates, the flow pattern wrapped around the inside of the cylinder. Figure 7(b) shows an example in a horizontal cylinder, photographed from above. The curved rope approaches the crown of the cylinder as the flow rate increases (Figure 7(b)(i)). At a critical flow rate, the crown is reached and some of the rope drains beyond the crown: the rope forms a Y-shape (Figure 7(b)(ii)). At higher flow rates, wraparound extends with almost linear rope boundaries. The narrowing of the flow pattern after it wraps around shows that surface tension dominates over downward momentum.

Wraparound in a horizontal cylinder is expected to occur when $Z_c \geq \pi D/4$ when the jet impinges normally at the midplane (see Figure 7(a)). Assuming $Z_c \approx R$, Equation [1] then predicts that wraparound will occur at flow rates above a critical value, $Q_{\text{wraparound}}$, given by

$$Q_{\text{wraparound}} = \left[\frac{\mu\gamma(1 - \cos \beta)}{\rho^2} \left(\frac{Z_c}{0.276} \right)^4 \right]^{1/3} \quad [4]$$

For the case shown in Figure 7(b), with $\beta = \pi/2$, wraparound is then expected where $Q \geq 4.7 \text{ dm}^3 \text{ min}^{-1}$, which is consistent with the observed transition in rope behaviour.

The area wetted by the cleaning liquid will be greater than that predicted by existing models when wraparound occurs. The increase in wetted area would be advantageous for applications where cleaning arises primarily from the chemical action of the cleaning liquid.

Impact of jet length and curvature on cleaning

Figure 8 shows the growth in the size of the cleaned region against time for layers of petroleum jelly on flat, vertical Perspex[®] walls cleaned with jets of three different lengths. The values of Q were chosen so that the jets had similar Q_{eff} values: Q_{eff} was estimated from measurements on clean walls. The presence of a soil layer affects the flow in the thin film beyond the cleaning front significantly: with the petroleum jelly a berm of dislodged soil collected at the cleaning front which deflected the thin film away from the surface and created a spray.

The cleaning profiles in Figure 8 are of similar form, with all data sets exhibiting rapid initial cleaning followed by an approach to an asymptote, denoted a_{max} . The asymptotic behaviour is associated with the soil having a yield stress. In each case a_{max} did not approach location of the film jump ($R = 36.9 \pm 2 \text{ mm}$ from experimental measurements on clean walls, see Figure 5). Bhagat and Wilson (2016) presented a detailed model of the flow in the RFZ, and gave results for two key transitions: r_b , where the growing viscous boundary layer reaches the surface, and r_t , the transition from laminar to turbulent flow in the film. For $d_N = 2 \text{ mm}$ and $Q_{\text{eff}} = 1.6 \text{ dm}^3 \text{ min}^{-1}$, their model gave $r_b = 12.3 \text{ mm}$ and $r_t = 15.2 \text{ mm}$, so a_{max} is estimated to lie in the region where the flow in the film is turbulent.

The data were fitted to the cleaning model reported by Glover *et al.* (2016) in their study of a different petroleum jelly, *viz.*

$$\frac{da}{dt} = \frac{K^5}{5a^4} \left[1 - \left(\frac{a}{a_{max}} \right)^4 \right] \quad a < a_{max} \quad [5]$$

where a is the radius of the cleaned region, K is the cleaning rate constant and t is time. For the case where $a = 0$ when $t = 0$, the growth of the cleaned region is given by

$$t = \frac{5}{4} \left(\frac{a_{max}}{K} \right)^5 \left[\ln \left(\frac{1 + \frac{a}{a_{max}}}{1 - \frac{a}{a_{max}}} \right) - 4 \left(\frac{a}{a_{max}} \right) + 2 \tan^{-1} \left(\frac{a}{a_{max}} \right) \right] \quad [6]$$

In the early stages of cleaning, $a \ll a_{max}$ and integrating Equation [5] gives

$$(a^5 - a_o^5)^{0.2} = K(t - t_o)^{0.2} \quad [7]$$

where a_o is the radius of the cleaned region when the cleaning front is first seen at time t_o .

The value of K was estimated by fitting the initial data to Equation [7] by eye. a_{max} was taken to be the maximum experimental value of $a + 1$ mm. All data sets had similar values of K and a_{max} , summarised in Table 4. The predictions from Equation [6] with these values are shown in Figure 8. The plots show that the cleaning profiles are not well described by the Glover *et al.* model. Feldung Damkjær *et al.* also reported that cleaning profiles obtained with petroleum jelly with longer jets deviated from the model behaviour. These results indicate that whilst Q_{eff} captures the effect of breakup and splatter on hydrodynamics, it does not give a complete description of the impact of the film dynamics on cleaning. Using Q_{eff} (based on S) tended to underestimate the rate: in this case it provides a useful engineering result and indicates that this topic requires further investigation.

Figure 9 shows the cleaning profiles obtained for Carbopol[®] layers applied to the inner wall of three of the vertical Perspex[®] cylinders alongside that obtained for a jet impinging on a similarly coated flat vertical wall. All four tests employed a coherent jet, so that the degree of splashing and jet breakup was similar. Under these conditions, wall curvature had little impact on cleaning dynamics, which is consistent with the observations on flow patterns.

Particular care had to be taken with the Carbopol[®] layers as the cleaning rate increased noticeably if they were left in contact with water, which is attributed to water diffusing into the layer and changing its rheology. The effect of soaking is demonstrated in Figure 10, which

shows that the approach to an asymptote, a_{\max} , was not observed at long times with the soaked layers. The fit of all three data sets to the expression $a = K t^{0.2}$ (see Wilson *et al.*, 2014), which Equation [5] collapses to when $a_{\max} \rightarrow \infty$, improves with soaking time. The K values (reflecting ease of cleaning) increased from 24.1 mm s^{0.2} (no soaking) to 29.1 (after 10 s) and 30.9 mm s^{0.2} (after 60 s), which is expected from the increased water content of the layer. Relating the value of K to the rheology of the layer is the subject of ongoing work.

The observed change in K (and a_{\max}) on soaking is important for industrial application. Soil in the lower regions of a tank is often contacted with cleaning liquid for extended times as a result of the falling film created by jets striking the wall above. The width of the cleaned region created by the passage of a jet will therefore increase with soaking time and this would suggest that for soaking-sensitive materials the jet would not have to make so many passes over the lower regions of a tank in order to clean it.

Conclusions

An experimental investigation of some of the factors influencing impinging water jet cleaning of vessel walls was conducted. The time taken to establish a steady flow pattern is short and can be estimated with some confidence from simple flow theory. The effect of jet length and wall curvature on the flow pattern and cleaning performance of impinging liquid jets has been investigated. Splatter arising from jet breakup and related phenomena was significant with non-coherent jets. The splatter data show a noticeable transition in behaviour as jet length increases.

Correcting the jet flow rate for losses due to splatter in existing models gave reasonable predictions for the shape of the radial flow zone. Correcting the flow rate in the film was not able to account for the differences observed in cleaning behaviour, but the splatter correction does provide an engineering estimate of the cleaning rate. The curvature of the wall had little effect on hydrodynamics and cleaning. The Carbopol[®] layers' cleaning behaviour changed on extended contact with water, which highlighted the need to understand how the soil interacts with the cleaning fluid.

Acknowledgements

Funding for MWLC from Newnham College, Cambridge, and a Commonwealth Scholarship for RKB are gratefully acknowledged, as is travel funding for DIW to attend the FCFP2018 conference from Jesus College, Cambridge, and assistance from Rubens Rosario Fernandes and Douglas Gibson. TVA, NT, SAW and RLW were all MEng research project students.

References

- Aouad, W., Landel, J.R., Davidson, J.F., Dalziel, S.B. and Wilson, D.I. (2016) Particle image velocimetry and modelling of horizontal coherent liquid jets impinging on and draining down a vertical wall, *Exp. Therm. Fluid Sci.*, **74**, 429-443.
- Bhagat, R.K. and Wilson, D.I. (2016) Flow in the thin film created by a coherent turbulent water jet impinging on a vertical wall, *Chem. Eng. Sci.*, **152**, 606-623.
- Bhagat, R.K., Perera, A.M. and Wilson, D.I. (2017) Cleaning tank walls by moving water jets: simple models and supporting experiments, *Food Bioprod. Proc.*, **102**, 31-54.
- Bhagat, R.K., Jha, N.K., Linden, P.F. and Wilson, D.I. (2018) On the origin of the hydraulic jump in a thin liquid film, *J. Fluid Mech.*, **851**, R5.
- Bhunia, S.K. and Lienhard J.H. (1994) Splattering during turbulent liquid jet impingement on solid targets, *J. Fluids Eng.*, **116**, 338-344.
- Bush, J.W. and Aristoff, J.M. (2003) The influence of surface tension on the circular hydraulic jump, *J. Fluid Mech.*, **489**, 229-238.
- Dinkgreve, M., Fazilati, M., Denn M.M. and Bonn, D. (2018) Carbopol: From a simple to a thixotropic yield stress fluid, *J. Rheo.*, **62**, 773-780.
- Eggers, J. and Villermaux, E. (2008) Physics of liquid jets, *Rep. Prog. Phys.*, **71**, 036601.
- Errico, M. (1986) A Study of the Interaction of Liquid Jets with Solid Surfaces, Ph.D. thesis, University of California, San Diego.
- Feldung Damkjær, N., Adler-Nissen, J., Jensen, B.B.B. and Wilson, D.I. (2017) Flow pattern and cleaning performance of a stationary liquid jet operating at conditions relevant for industrial tank cleaning, *Food Bioprod. Proc.*, **101**, 145-156.
- Fuchs, E., Helbig, M., Pfister, M. and Majschak, J.P. (2017) Increasing the cleaning efficiency of the cleaning-in-place method by applying discontinuous liquid jets, *Chemie Ingenieur Technik*, **89**, 1072-1082.
- Glover, H.W, Brass, T, Bhagat, R.K, Davidson, J. F, Pratt, L. and Wilson, D.I. (2016) Cleaning of complex soil layers on vertical walls by fixed and moving impinging liquid jets, *J. Food Eng.*, **178**, 95-109.

- 495 Lienhard, J.H., Liu, X. and Gabour, L.A. (1992) Splattering and heat transfer during
496 impingement of a turbulent liquid jet, *J. Heat Transfer*, **114**, 362-372.
- 497 Lin, S.P. and Reitz, R.D. (1998) Drop and spray formation from a liquid jet, *Annual Review of*
498 *Fluid Mechanics*, **30**, 85-105.
- 499 Nusselt, W. (1916) Die oberflächenkondensation des wasserdampfes, *Z. Ver. Dtsch. Ing.*, **60**,
500 **541-546 and 569-575**.
- 501 Wang, T., Faria, D., Stevens, L.J., Tan, J.S.C., Davidson, J.F. and Wilson, D.I. (2013) Flow
502 patterns and draining films created by horizontal and inclined water jets impinging on
503 vertical walls, *Chem. Eng. Sci.*, **102**, 585-601.
- 504 Watson, E.J. (1964) The radial spread of a liquid jet over a horizontal plane, *J. Fluid Mech.*,
505 **20**, 481-499.
- 506 Wilson, D.I., He, B.L., Dao, H.D.A, Lai, K.Y., Morison, K.R. and Davidson, J.F. (2012)
507 Surface flow and drainage films created by horizontal impinging liquid jets, *Chem. Eng.*
508 *Sci.*, **68**, 449-460.
- 509 Wilson, D.I., Atkinson, P., Köhler, H., Mauermann, M., Stoye, H., Suddaby, K., Wang, T.,
510 Davidson, J.F. and Majschak, J-P. (2014) Cleaning of soft-solid soil layers on vertical and
511 horizontal surfaces by coherent impinging liquid jets, *Chem. Eng. Sci.*, **109**, 183-196.

512

513 Nomenclature

514 Roman

515	a	radius of cleaned area	m
516	a_o	radius of cleaned area when cleaning front is first seen	m
517	a_{\max}	radius of cleaned area, asymptotic value	m
518	B	rope width	m
519	C	chord length	m
520	d_N	nozzle diameter	m
521	D	cylinder inner diameter	m
522	g	gravitational acceleration	m s^{-2}
523	K	cleaning rate constant	$\text{m s}^{-0.2}$
524	L	horizontal distance from nozzle to target	m
525	\dot{m}	mass flow rate leaving nozzle	kg s^{-1}
526	Q	volumetric flow rate through the nozzle	$\text{m}^3 \text{s}^{-1}$
527	Q_{eff}	volumetric flow rate in the falling film	$\text{m}^3 \text{s}^{-1}$
528	$Q_{\text{wraparound}}$	volumetric flow rate above which wraparound is expected to occur	$\text{m}^3 \text{s}^{-1}$
529	r	distance in radial direction	m
530	r_b	radius where the boundary layer reaches the surface in the RFZ	m
531	r_o	jet radius	m
532	r_t	transition radius from laminar to turbulent flow in the RFZ	m
533	R	half-width of the RFZ at the level of the point of impingement	m
534	R_c	half-width of the wetted region at the level of the point of impingement	m
535	Re	Reynolds number	-
536	S	splatter fraction	-
537	t	time	s
538	t_o	time at which cleaning front of radius a_o is first seen	s
539	t_B	duration of jet burst	s
540	t_E	time taken to establish RFZ	s
541	U	mean velocity of liquid film	m s^{-1}
542	U_o	jet velocity	m s^{-1}
543	We	Weber number	-
544	x	distance in horizontal direction	m
545	y	estimate of length of interest	m

546	Y	length of interest	m
547	z	distance in vertical direction	m
548	Z	height of the film jump	m
549	Z_c	height of the top of the rope	m
550			
551	Greek		
552	β	solid-liquid contact angle	rad.
553	γ	vapour-liquid surface tension	N m ⁻¹
554	θ	angular position on liquid film	rad.
555	κ	wall curvature	m ⁻¹
556	μ	liquid dynamic viscosity	Pa s
557	ν	liquid kinematic viscosity	m ² s ⁻¹
558	ρ	liquid density	kg m ⁻³
559	ϕ	jet impingement angle	rad.
560	ψ	angle of the liquid film from the point of impingement	rad.
561	Ψ	angle of the second camera from the point of impingement	rad.
562			
563	Acronyms		
564	CIP	cleaning-in-place	
565	PMMA	polymethylmethacrylate	
566	RFZ	radial flow zone	
567			

Appendix A – Correction for refraction

The curvature of the cylinders affects the extraction of dimensions from photographs: R and R_c in vertical cylinders, and Z and Z_c in horizontal cylinders.

A second camera was moved around the apparatus to obtain refraction-free images so that the dimension of interest could be read directly off the graticule tape. To ensure that the camera was aligned normal to the surface of the cylinder, pairs of calibration lines showing the diameter of the cylinder were drawn at 10° intervals on the outer surface of the cylinder, shown in Figure A1.

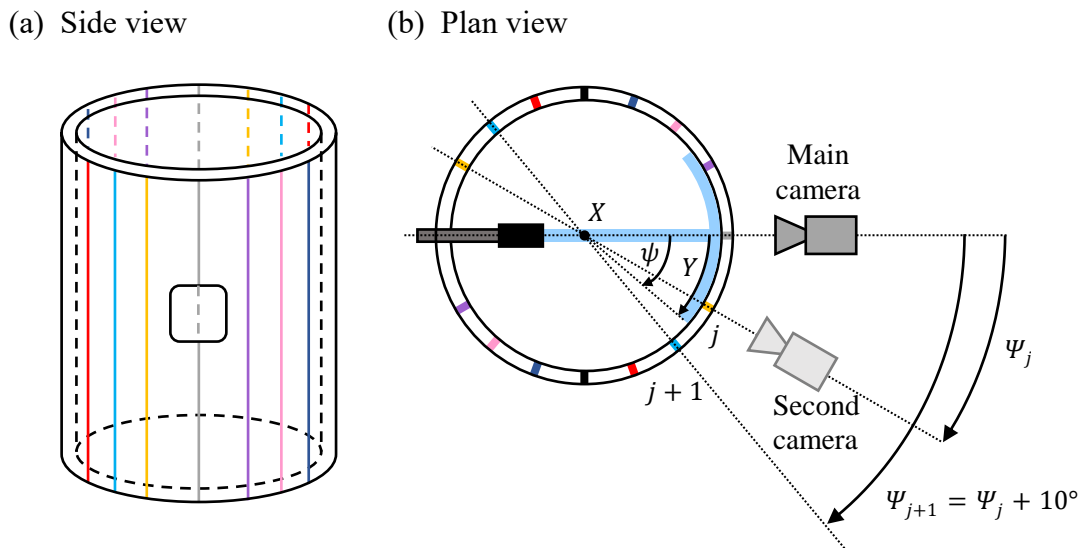


Figure A1 Schematic of a vertical cylinder showing calibration lines: (a) side view, and (b) plan view. ψ and Ψ are the angles of liquid film and second camera from the point of impingement, respectively. X is the axis of the cylinder. Position of calibration lines not drawn to scale: in this case the second camera is positioned at j .

The experimental set up is limited in that the second camera can only be positioned accurately at 10° intervals, labelled Ψ , from the point of impingement. It does, however, remove the uncertainty in judging the exact position of the water film by eye. To obtain an estimate of the measurement from the second camera, a harmonic weighting was used

$$Y = \frac{\left[y_j * \frac{1}{|\psi_j - \Psi_j|} \right] + \left[y_{j+1} * \frac{1}{|\psi_{j+1} - \Psi_{j+1}|} \right]}{\left[\frac{1}{|\psi_j - \Psi_j|} + \frac{1}{|\psi_{j+1} - \Psi_{j+1}|} \right]} \quad [\text{A1}]$$

where the estimate of the length of interest, Y , and its angle ψ , are y_j and ψ_j at position j , respectively; these are y_{j+1} and ψ_{j+1} at the next position ($j + 1$).

The estimates from the second camera were plotted against the chord length measured using the main camera, C , scaled by the wall curvature, κ (Figure A2). A second order polynomial was found to give the best fit to the experimental data (see Table A1). Measurements of R and R_c on vertical cylinders and Z and Z_c on horizontal cylinders were obtained using only the main camera and this calibration.

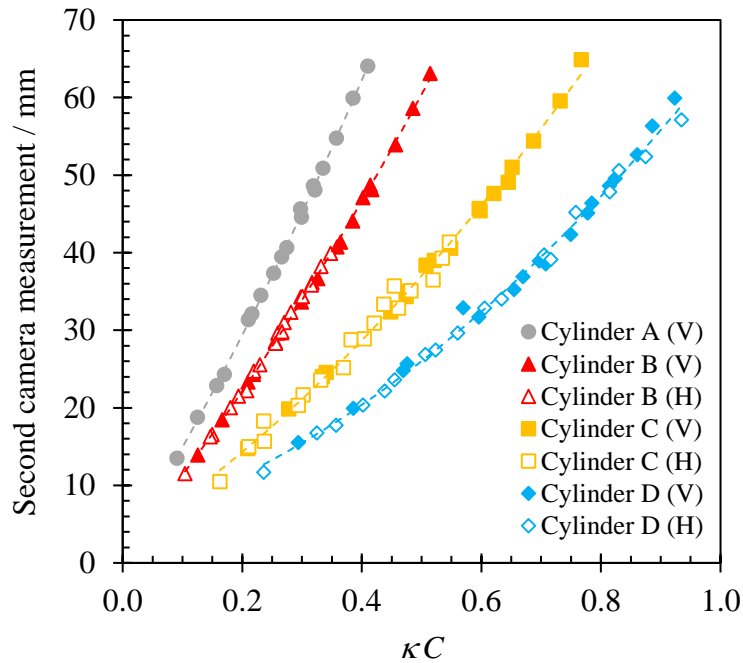


Figure A2 Fit of empirical correlations (Table A1) to experimental data. Error bars omitted for clarity. (V): R and R_c on vertical cylinders, and (H): Z and Z_c on horizontal cylinders.

614

615 Table A1 Empirical correlations used to correct for refraction, where $m = R, R_c, Z$ or Z_c .

Cylinder	Curvature, κ / m^{-1}	Correlation	Regression coefficient
A	6.9	$m = 66.1 (\kappa C)^2 + 124.9 (\kappa C) + 1.74$	0.9992
B	9.1	$m = 49.2 (\kappa C)^2 + 93.1 (\kappa C) + 1.55$	0.9989
C	14	$m = 38.2 (\kappa C)^2 + 49.0 (\kappa C) + 2.97$	0.9944
D	20	$m = 36.2 (\kappa C)^2 + 23.8 (\kappa C) + 5.07$	0.9947

616

617

Appendix B – Estimate of time taken to establish the initial jump

Wilson *et al.* (2012) presented an approximate model for the flow in thin radial film in the RFZ in the steady state, which yielded the estimate of R via Equation [1]. The mean velocity in the film, U , at radial position r was given by

$$\frac{1}{U} \approx \frac{1}{U_o} + \frac{10\pi^2 \rho \mu}{3\dot{m}^2} (r^3 - r_o^3) \quad [\text{B1}]$$

where r_o is the radius of the jet and $\dot{m} = \rho Q$ is the mass flow rate leaving the nozzle. Using this result to describe the mean velocity in the growing film and setting

$$U = \frac{dr}{dt} \quad [\text{B2}]$$

allows the time for the liquid to reach the location of the jump to be estimated from

$$\int_0^{t_E} dt = \int_{r_o}^R \frac{dr}{U} \quad [\text{B3}]$$

Substituting [B1] into [B3], assuming $1/U_o \approx 0$ and $r^3 \gg r_o^3$, integrating, setting $R^4 \gg r_o^4$ and using the expression for R from Equation [1] gives

$$t_E = \frac{0.276^4}{4} \frac{10\pi^2}{3} \frac{\dot{m}}{\gamma(1 - \cos\beta)} \quad [\text{B4}]$$

For high flow rate jets, the wall has a weak influence on R , suggesting $\cos\beta \approx 0$ (Bhagat and Wilson, 2016), yielding

$$t_E = 0.0477 \frac{\dot{m}}{\gamma} \quad [\text{B5}]$$

The surface tension of water at 20°C is 0.074 N m⁻¹, giving $t_E = 0.65\dot{m}$. For the case in Figure 2, $\dot{m} = 2 \text{ kg min}^{-1}$ and $t_E = 20 \text{ ms}$.

Bhagat and Wilson (2016) presented a more detailed model for the velocity in the thin film. Employing this in the above derivation yields

$$t_E = \frac{8}{U_o} \left[0.125r + \frac{2.12r^{5/2}}{5(2r_o)^{3/2}\sqrt{Re}} \right]_{r_o}^{0.48r_o Re^{1/3}} + \frac{8}{U_o} \left[0.1975r + \frac{3.792r^4}{4(2r_o)^3 Re} \right]_{0.48r_o Re^{1/3}}^{0.5928r_o Re^{1/3}} + \frac{1}{U_o} \left[(2.37 - 0.0108\sqrt{Re})r + \frac{0.668r^{13/4}}{13(2r_o)^{9/4} Re^{1/4}} \right]_{0.5928r_o Re^{1/3}}^R \quad [\text{B6}]$$

Tables

Table 1 Summary of experimental conditions used to investigate the effect of jet length.

	d_N		
	2 mm	3 mm	4 mm
$Q / \text{dm}^3 \text{min}^{-1}$	0.8 – 3.5	0.8 – 5.5	1.0 – 7.0
$U_o / \text{m s}^{-1}$	4.2 – 18.6	1.9 – 13.0	1.3 – 9.3
L / m	0.06 – 1	0.06 – 1	0.06 – 1
Re	8 500 – 37 000	5 700 – 39 000	5 300 – 37 000
We	480 – 9 300	140 – 6 800	95 – 4 700

Table 2 Dimensions of the Perspex[®] cylinders used.

Cylinder	Inner diameter, D / mm	Wall thickness / mm	Curvature, κ / m^{-1}
A	290	5	6.9
B	220	5	9.1
C	138	6	14
D	100	5	20

Table 3 Summary of experimental conditions used to investigate the effect of wall curvature.

	d_N		
	2 mm	2 mm	4 mm
$Q / \text{dm}^3 \text{min}^{-1}$	0.4 – 2.0	0.4 – 2.0	4.0 – 7.0
$U_o / \text{m s}^{-1}$	2.1 – 11	2.1 – 11	5.3 – 9.3
L / m	0.07	0.03	0.03
Re	4 200 – 21 000	4 200 – 21 000	21 000 – 37 000
We	120 – 3 000	120 – 3 000	1 500 – 4 700
Target	Flat wall	Cylinders A – D	Cylinder D

Table 4 Summary of the Glover *et al.* (2016) model parameters obtained from the experimental data shown in Figure 8.

L / mm	K / mm s ^{-0.2}	a_{\max} / mm
60	9.8 ± 1.1	19.3
245	8.6 ± 1.2	18.5
350	8.3 ± 1.9	18.6

List of Figures

- Figure 1 Schematic of phenomena affecting the flow pattern and cleaning performance of a long liquid jet in a tank cleaning application. Q is the flow rate at the nozzle and L is the distance travelled by the jet. Droop and breakup can cause the angle of impingement ϕ to differ from that for a direct path.
- Figure 2 Flow pattern created by normal jet impinging on a flat vertical Perspex[®] wall, $d_N = 2$ mm, $Q = 2$ dm³ min⁻¹, and $L = 70$ mm. (a) Steady pattern, showing key dimensions – subscript c refers to external edge of the rope. (b) Evolution of flow pattern following initial impingement by a steady jet. Horizontal loci indicate steady state values.
- Figure 3 Comparison of predictions of the RFZ formation time, t_E , with experimental measurements obtained for a coherent water jet at 20°C impinging on a flat vertical glass wall, $d_N = 2.67$ mm. The growth of the thin film was analysed in the three different directions indicated on the inset sketch: the average value \pm standard error is plotted.
- Figure 4 Effect of (a) jet Reynolds number, and (b) L , on measured splatter fraction. Symbols defined in legend: symbol shape indicates jet length while open symbols indicate that jet breakup was observed. For clarity, data in (b) are offset on the y-axis in order of nozzle diameter and error bars are omitted. Data sets for $d_N = 2$ mm are shown in blue in the colour version of this Figure.
- Figure 5 Comparison of measured half-width of the radial flow zone at the level of the point of impingement, R , with the Wilson *et al.* (2012) model (Equation [1]). Data plotted against flow rate in film, Q_{eff} . Inset shows correlation between height Z and R , $Z \approx 4R/5$. Dashed line shows line of equality, $Z = R$. Data sets for $d_N = 2$ mm are shown in blue in the colour version of this Figure.
- Figure 6 Effect of flow rate on (a) Z , and (b) R , for a coherent horizontal water jet ($d_N = 2$ mm) impinging normally on (i) vertical cylinders, and (ii) horizontal

cylinders. Error bars omitted for clarity: these are approximately ± 2 mm for Z , ± 2 mm for R and ± 0.1 dm³ min⁻¹ for Q .

Figure 7 (a) Shedding from the rope ($Q = 4.5$ dm³ min⁻¹), and (b) plan view of a horizontal jet impinging normally on a horizontal cylinder. Flow rate increases from (i) to (iv). $d_N = 4$ mm, $L = 30$ mm and $\kappa = 20$ m⁻¹. Vertical black line in (b) indicates the crown (top) of the cylinder.

Figure 8 Evolution of the cleaned region radius over time for 0.2 mm thick petroleum jelly layers on flat walls. Conditions: $d_N = 2$ mm, $Q_{\text{eff}} = 1.6$ dm³ min⁻¹ for $L = 60, 245$ and 350 mm. Note log₁₀ time scale. Loci show fit to Equation [6]. Error bars omitted for clarity: these are approximately ± 2 mm for a .

Figure 9 Effect of curvature on size of cleaned region for 1.3 mm thick Carbopol[®] layers on vertical cylinders. Coherent jet, $d_N = 2.0$ mm, $Q_{\text{eff}} = 1.0$ dm³ min⁻¹, no soaking. Note log₁₀ time scale. Error bars omitted for clarity: these are approximately ± 2 mm for a .

Figure 10 Effect of soaking time on the removal of 0.2 mm thick Carbopol[®] layers on flat walls. A thin film of water covered the wall for 0 s (no soaking), 10 s or 60 s. In these tests the target wall was horizontal rather than vertical, and the jet was vertical rather than horizontal, as this allowed the soil to be cleaned directly after soaking. Conditions: $d_N = 2$ mm, $Q = 2$ dm³ min⁻¹ and $L = 245$ mm. Loci show fit to the expression $a = K t^{0.2}$. Error bars omitted for clarity: these are approximately ± 2 mm for a .

List of Supplementary Figures

Figure S1 Data in Figure 4(b) plotted against L/d_N . Error bars omitted for clarity. Data sets for $d_N = 2$ mm are shown in blue in the colour version of this Figure.

Figure S2 Splatter fraction estimated from the Q_{eff}/Q data reported by Feldung Damkjær *et al.* (2017) for industrial nozzles and long jet travel distances. Error bars are not shown as no attempt was made to quantify the errors. Data sets for $d_N = 3.8$ mm are shown in blue in the colour version of this Figure.

Figure S3 Comparison of measured half-width of the radial flow zone at the level of the point of impingement, R , with measured half-width of the wetted region at the level of the point of impingement, R_c . Dashed line shows line of $R_c = 4R/3$. Data sets for $d_N = 2$ mm are shown in blue in the colour version of this Figure.

Figure S4 Effect of wall curvature on the width of the rope, $B(0)$, at the top of the RFZ and at the level of the impingement point, $B(\pi/2)$. Also plotted are the loci for the model for B presented by Wang *et al.* (2013). Conditions: coherent jets, $d_N = 2.0$ mm. Error bars omitted for clarity: these are approximately ± 2 mm for B and $\pm 0.1 \text{ dm}^3 \text{ min}^{-1}$ for Q .

Figures

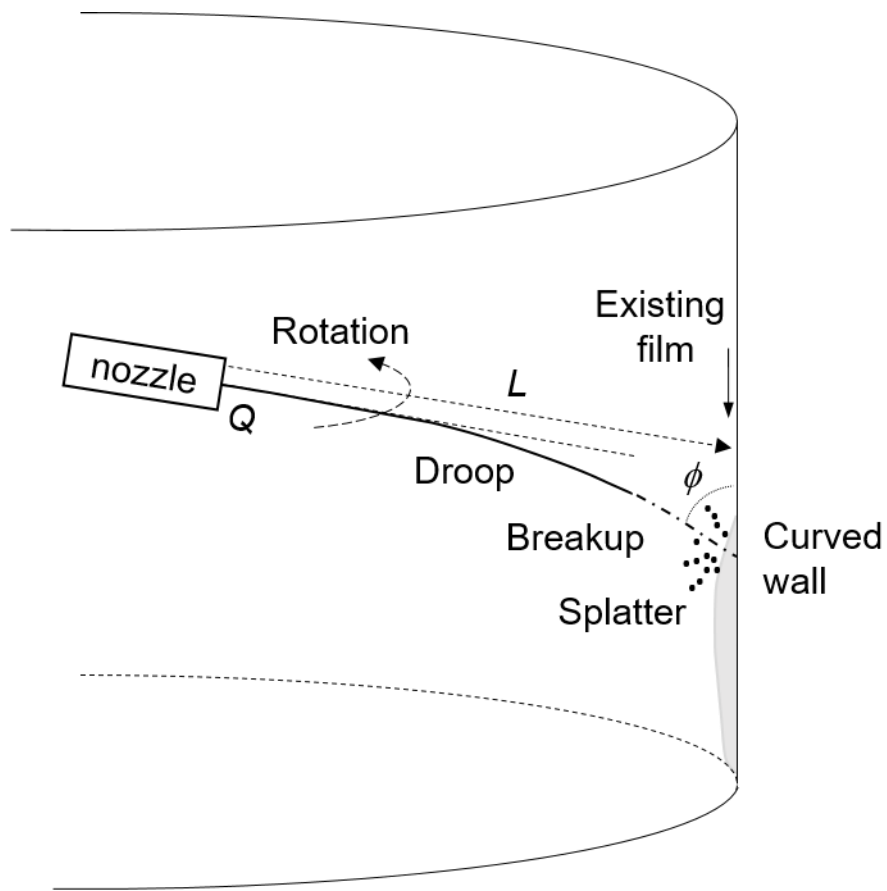
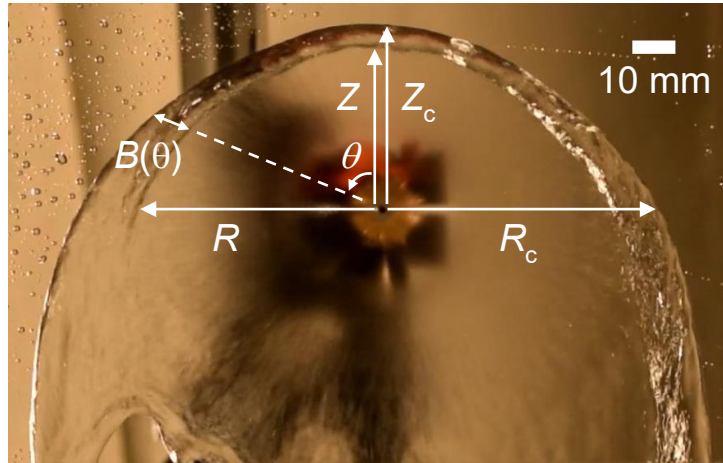


Figure 1 Schematic of phenomena affecting the flow pattern and cleaning performance of a long liquid jet in a tank cleaning application. Q is the flow rate at the nozzle and L is the distance travelled by the jet. Droop and breakup can cause the angle of impingement ϕ to differ from that for a direct path.

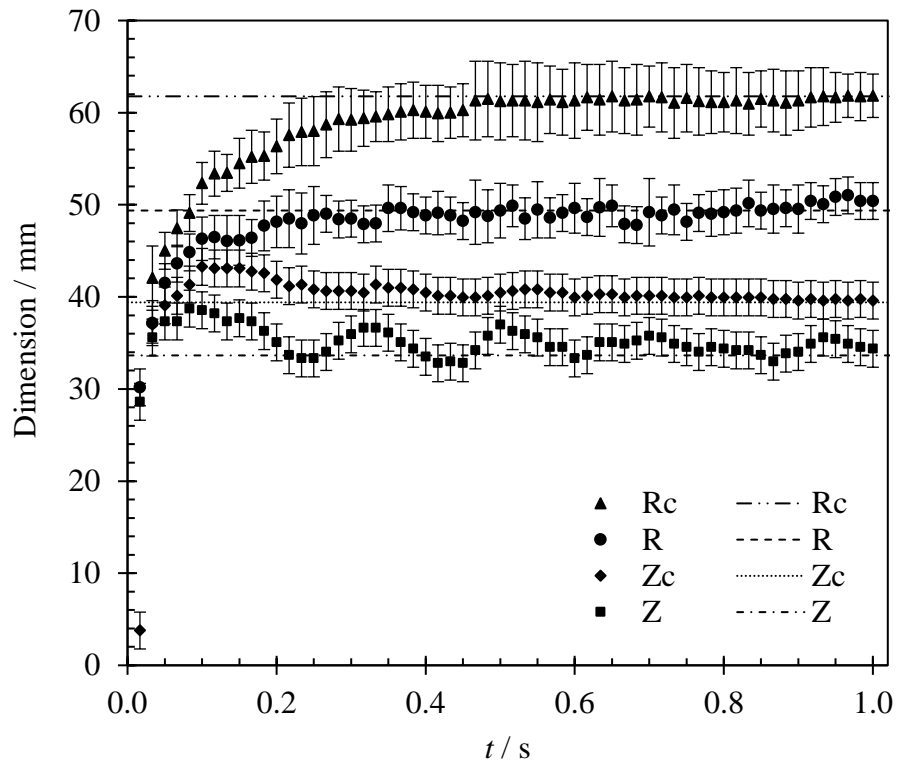
742 (a)



743

744

745 (b)



746

747

748 Figure 2 Flow pattern created by normal jet impinging on a flat vertical Perspex[®] wall,
 749 $d_N = 2$ mm, $Q = 2$ dm³ min⁻¹, and $L = 70$ mm. (a) Steady pattern, showing key
 750 dimensions – subscript c refers to external edge of the rope. (b) Evolution of flow
 751 pattern following initial impingement by a steady jet. Horizontal loci indicate
 752 steady state values.

753

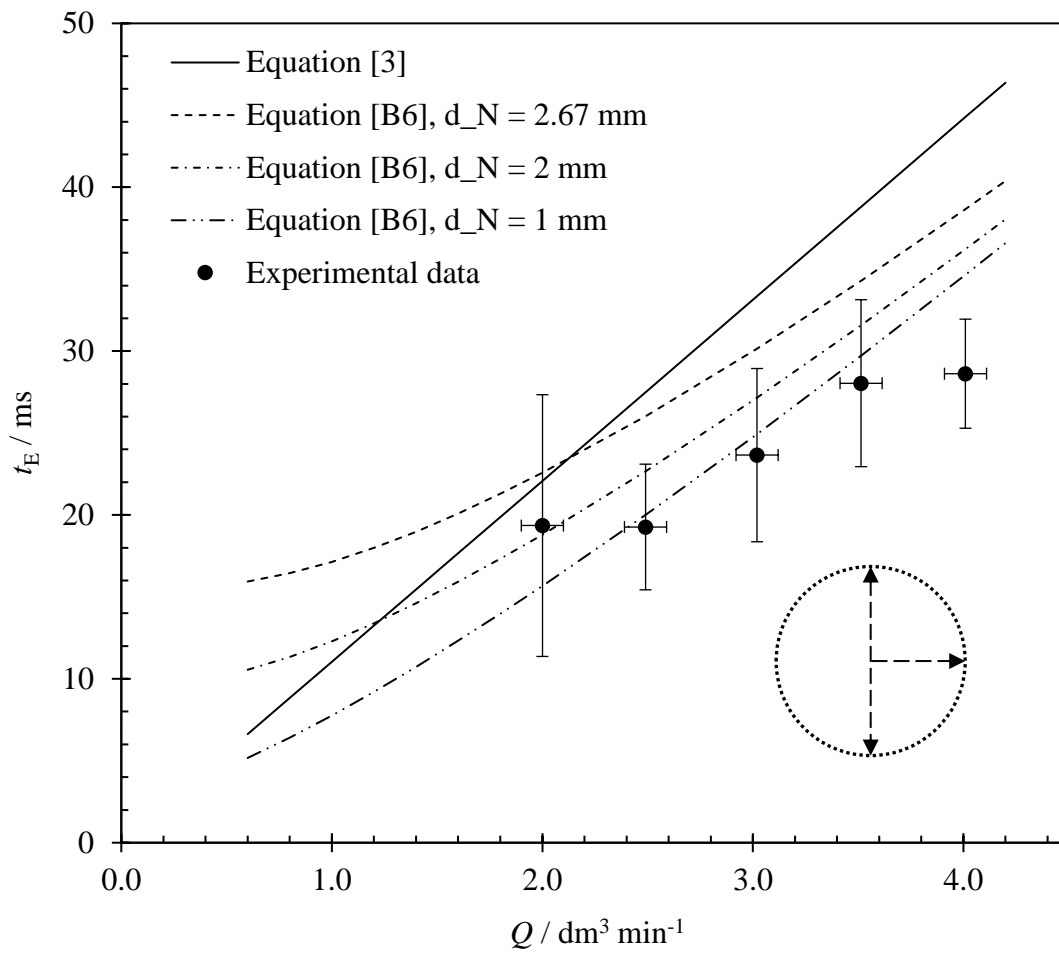
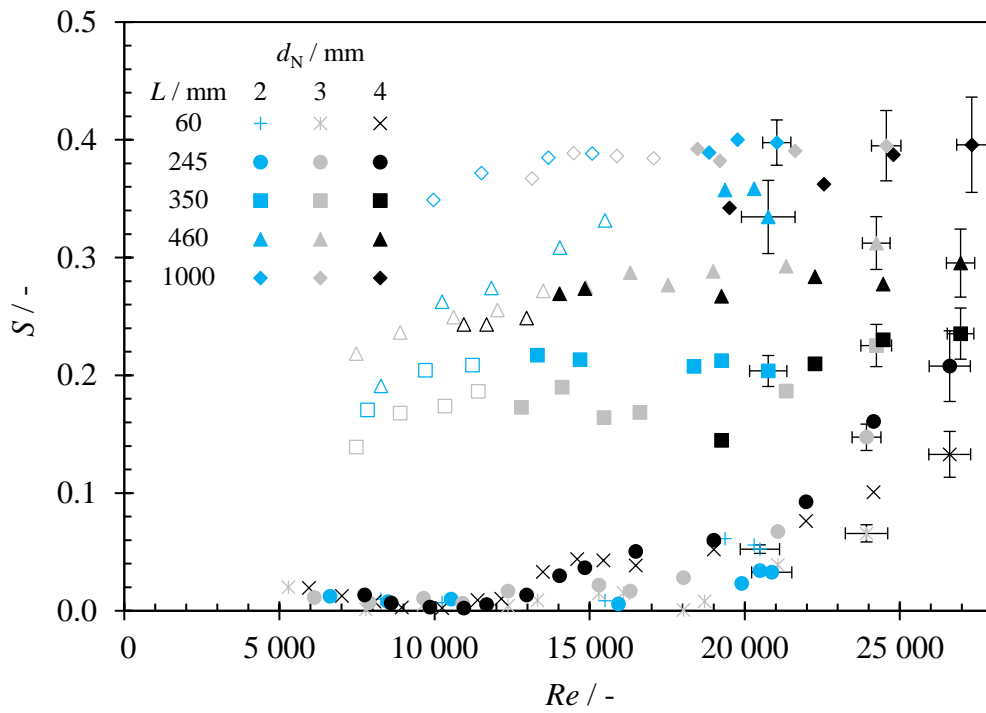


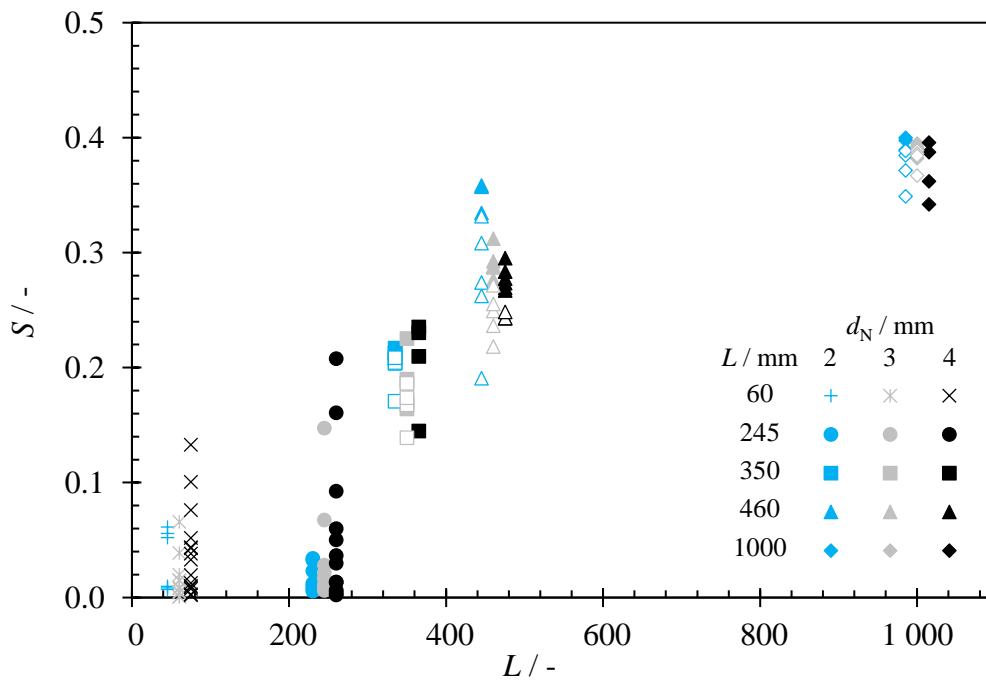
Figure 3 Comparison of predictions of the RFZ formation time, t_E , with experimental measurements obtained for a coherent water jet at 20°C impinging on a flat vertical glass wall, $d_N = 2.67$ mm. The growth of the thin film was analysed in the three different directions indicated on the inset sketch: the average value \pm standard error is plotted.

763 (a)



764

765 (b)



766

767

768 Figure 4 Effect of (a) jet Reynolds number, and (b) L , on measured splatter fraction.

769 Symbols defined in legend: symbol shape indicates jet length while open symbols

770 indicate that jet breakup was observed. For clarity, data in (b) are offset on the y-

771 axis in order of nozzle diameter and error bars are omitted. Data sets for $d_N = 2$ mm

772 are shown in blue in the colour version of this Figure.

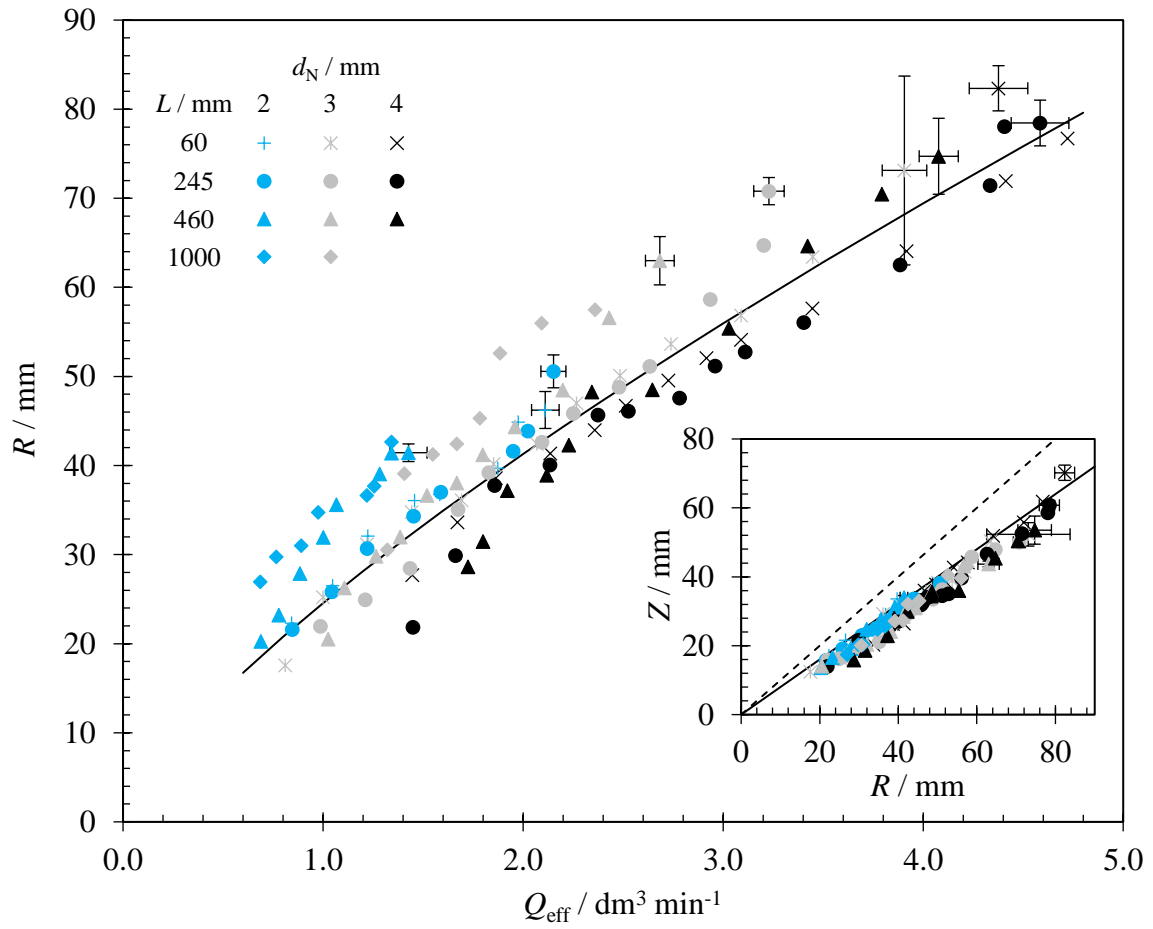


Figure 5 Comparison of measured half-width of the radial flow zone at the level of the point of impingement, R , with the Wilson *et al.* (2012) model (Equation [1]). Data plotted against flow rate in film, Q_{eff} . Inset shows correlation between height Z and R , $Z \approx 4R/5$. Dashed line shows line of equality, $Z = R$. Data sets for $d_N = 2 \text{ mm}$ are shown in blue in the colour version of this Figure.

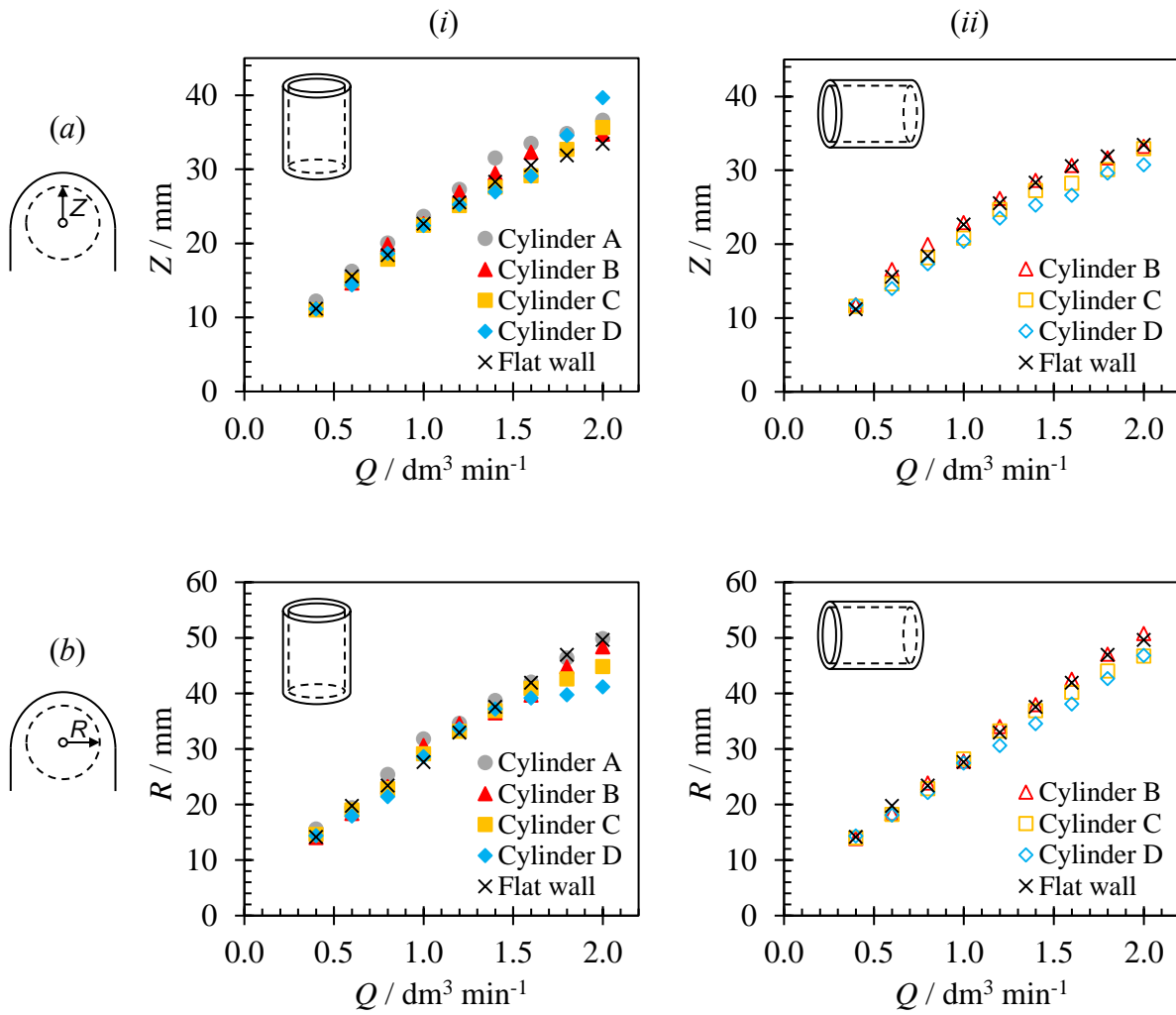
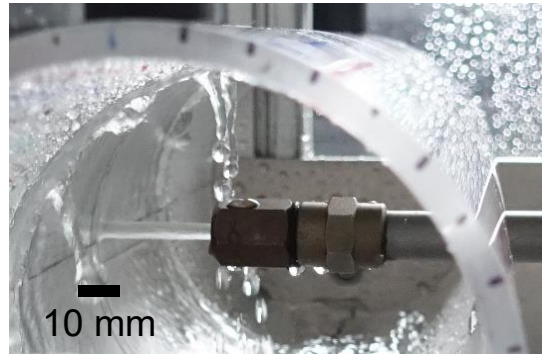


Figure 6 Effect of flow rate on (a) Z , and (b) R , for a coherent horizontal water jet ($d_N = 2 \text{ mm}$) impinging normally on (i) vertical cylinders, and (ii) horizontal cylinders. Error bars omitted for clarity: these are approximately $\pm 2 \text{ mm}$ for Z , $\pm 2 \text{ mm}$ for R and $\pm 0.1 \text{ dm}^3 \text{ min}^{-1}$ for Q .

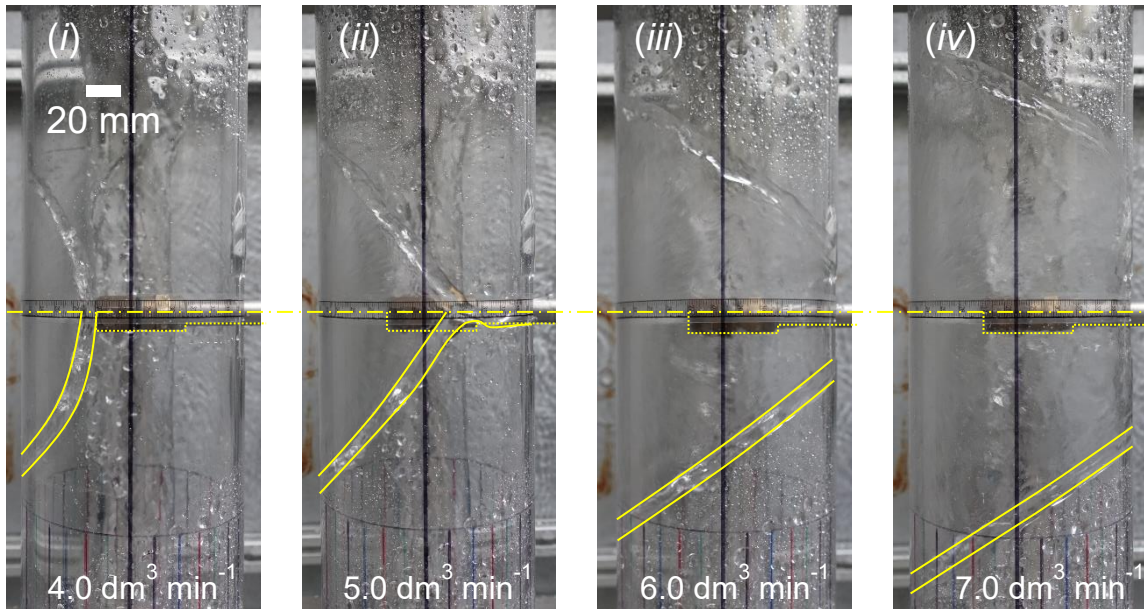
795 (a)



796

797

798 (b)



799

800

801 **Figure 7** (a) Shedding from the rope ($Q = 4.5 \text{ dm}^3 \text{ min}^{-1}$), and (b) plan view of a horizontal
 802 jet impinging normally on a horizontal cylinder. Flow rate increases from (i) to (iv).
 803 $d_N = 4 \text{ mm}$, $L = 30 \text{ mm}$ and $\kappa = 20 \text{ m}^{-1}$. **Vertical black line** in (b) indicates the
 804 crown (top) of the cylinder.

805

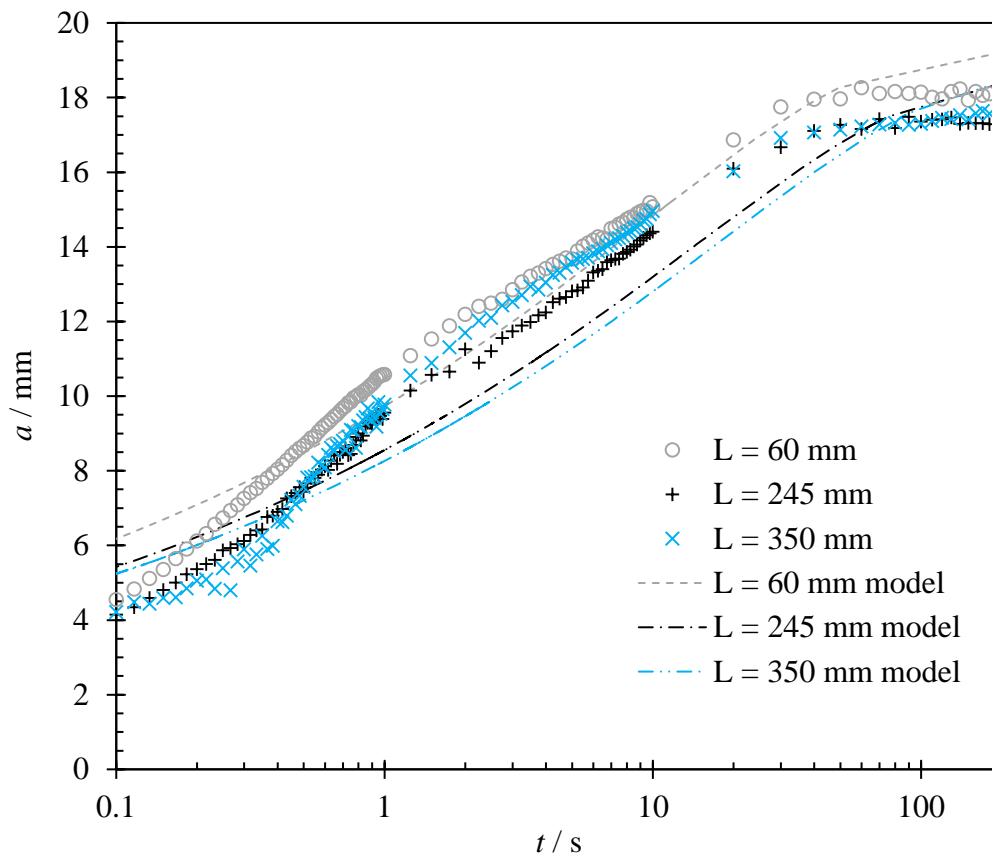


Figure 8 Evolution of the cleaned region radius over time for 0.2 mm thick petroleum jelly layers on flat walls. Conditions: $d_N = 2$ mm, $Q_{\text{eff}} = 1.6 \text{ dm}^3 \text{ min}^{-1}$ for $L = 60, 245$ and 350 mm. Note \log_{10} time scale. Loci show fit to Equation [6]. Error bars omitted for clarity: these are approximately ± 2 mm for a .

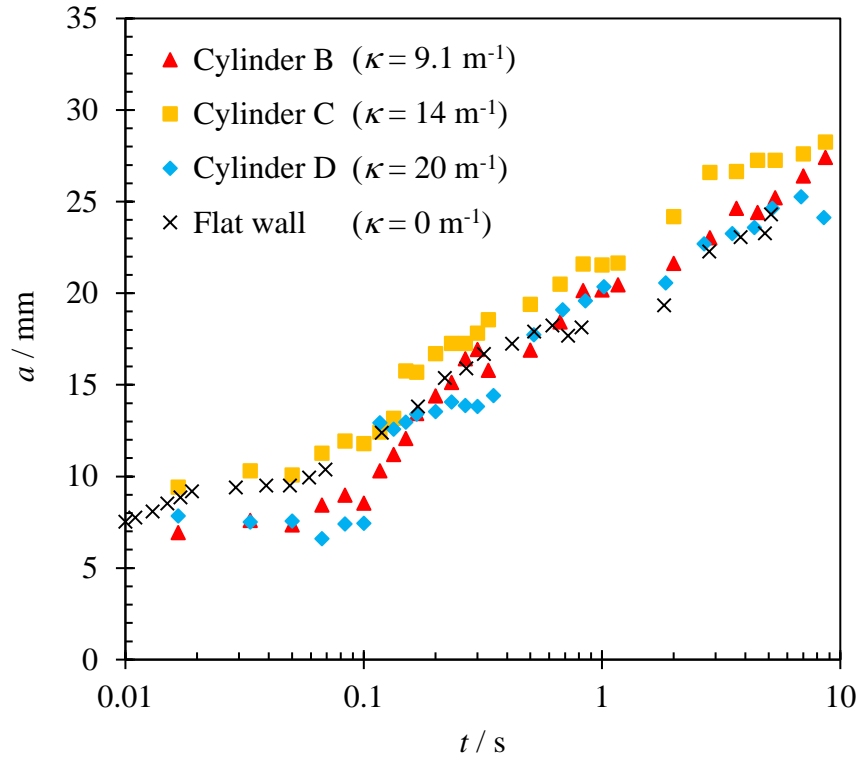


Figure 9 Effect of curvature on size of cleaned region for 1.3 mm thick Carbopol® layers on vertical cylinders. Coherent jet, $d_N = 2.0$ mm, $Q_{\text{eff}} = 1.0 \text{ dm}^3 \text{ min}^{-1}$, no soaking. Note \log_{10} time scale. Error bars omitted for clarity: these are approximately ± 2 mm for a .

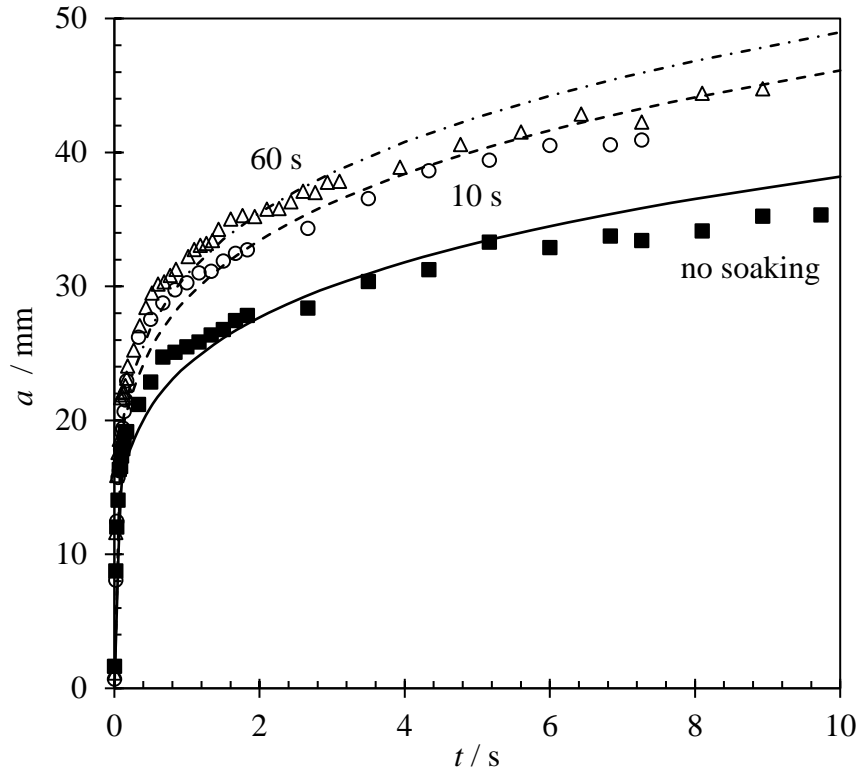


Figure 10 Effect of soaking time on the removal of 0.2 mm thick Carbopol[®] layers on flat walls. A thin film of water covered the wall for 0 s (no soaking), 10 s or 60 s. In these tests the target wall was horizontal rather than vertical, and the jet was vertical rather than horizontal, as this allowed the soil to be cleaned directly after soaking. Conditions: $d_N = 2$ mm, $Q = 2$ dm³ min⁻¹ and $L = 245$ mm. Loci show fit to the expression $a = K t^{0.2}$. Error bars omitted for clarity: these are approximately ± 2 mm for a .

Supplementary Figures

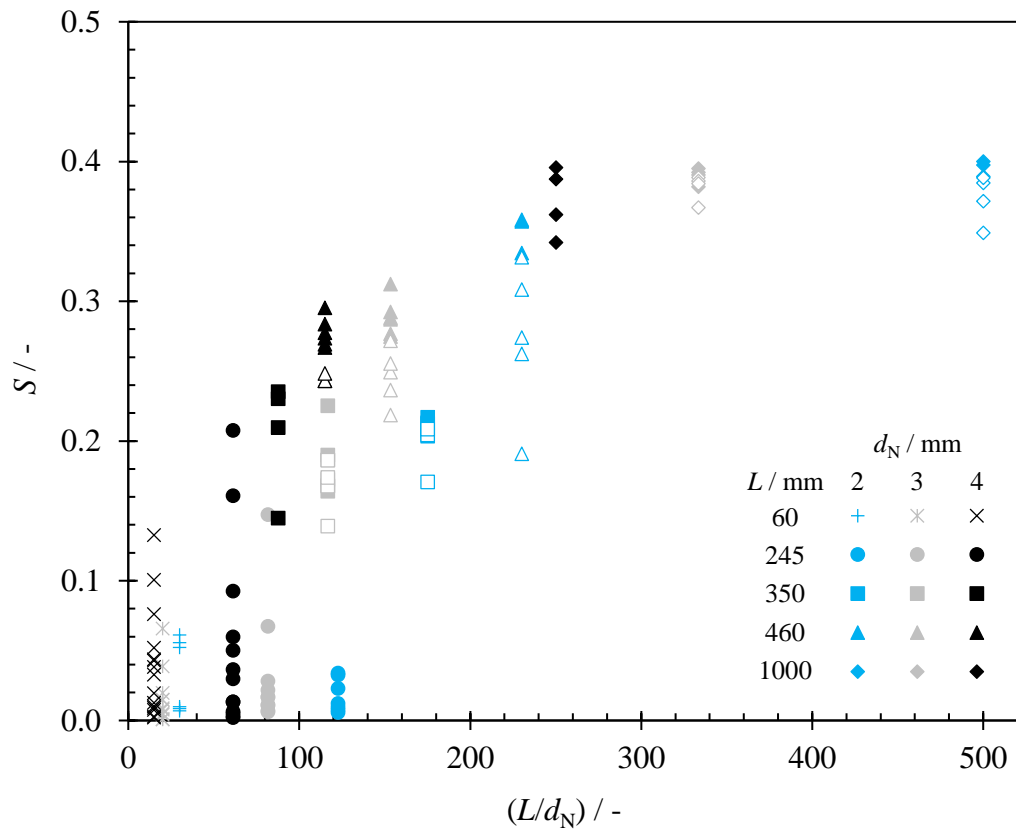
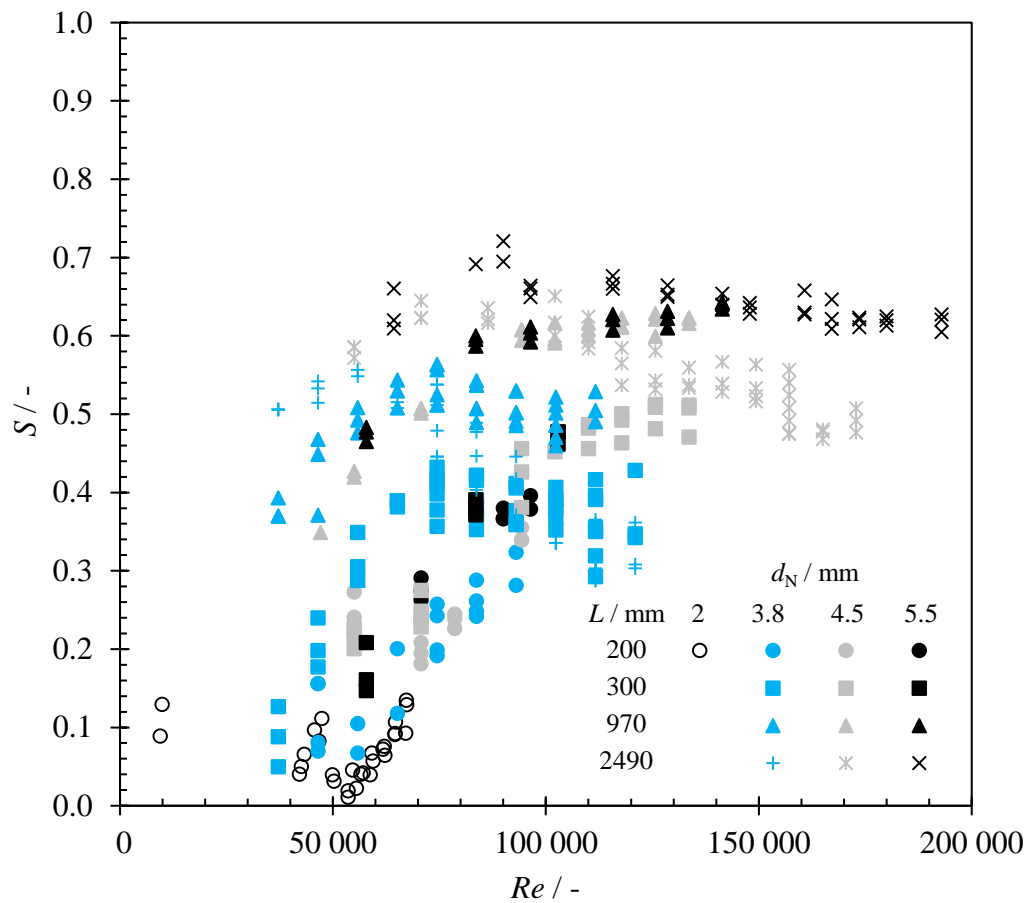


Figure S1 Data in Figure 4(b) plotted against L/d_N . Error bars omitted for clarity. Data sets for $d_N = 2 \text{ mm}$ are shown in blue in the colour version of this Figure.

841



842

843

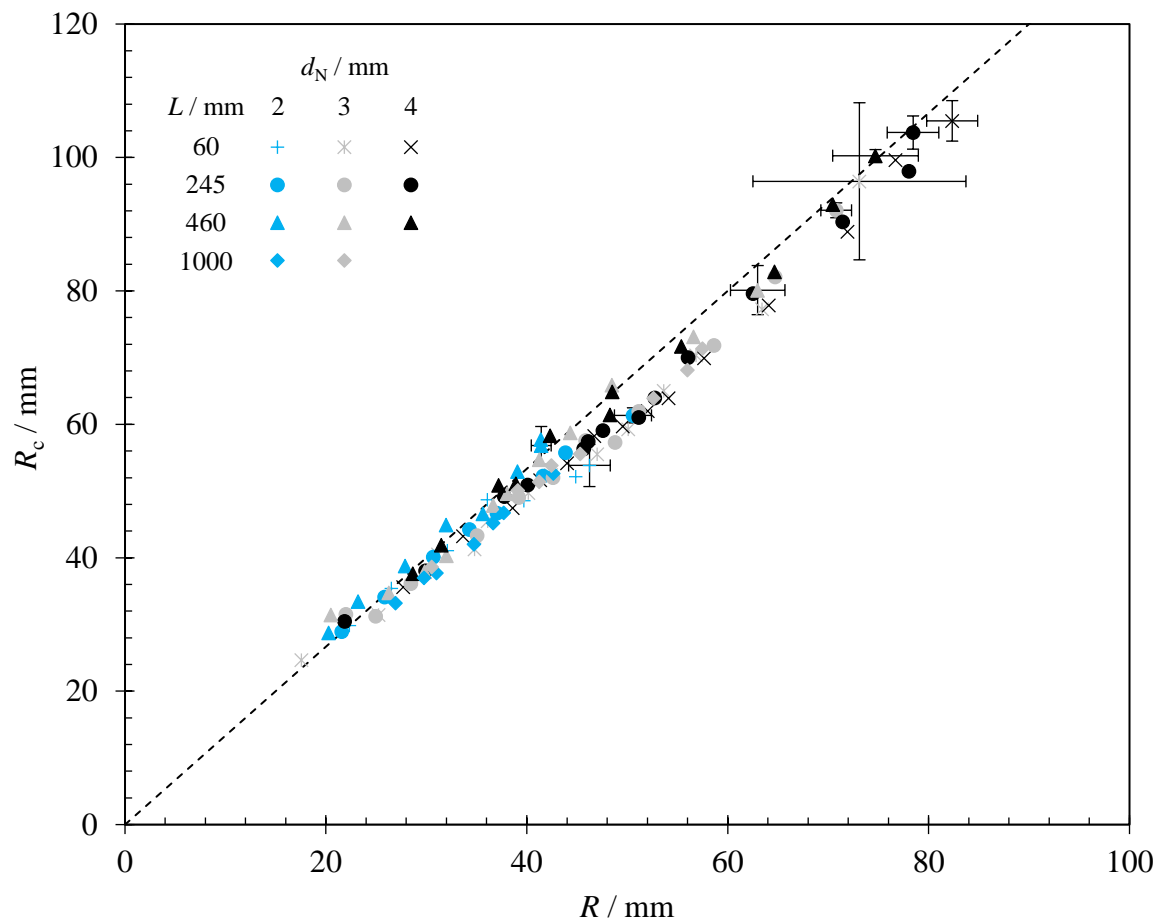
844 **Figure S2** Splatter fraction estimated from the Q_{eff}/Q data reported by Feldung Damkjær *et*
 845 *al.* (2017) for industrial nozzles and long jet travel distances. Error bars are not
 846 shown as no attempt was made to quantify the errors. Data sets for $d_N = 3.8$ mm
 847 are shown in blue in the colour version of this Figure.

848

849

850

851



852

853

854 **Figure S3** Comparison of measured half-width of the radial flow zone at the level of the point
 855 of impingement, R , with measured half-width of the wetted region at the level of
 856 the point of impingement, R_c . Dashed line shows line of $R_c = 4R/3$. **Data sets for**
 857 $d_N = 2$ mm are shown in blue in the colour version of this Figure.

858

859

860

861

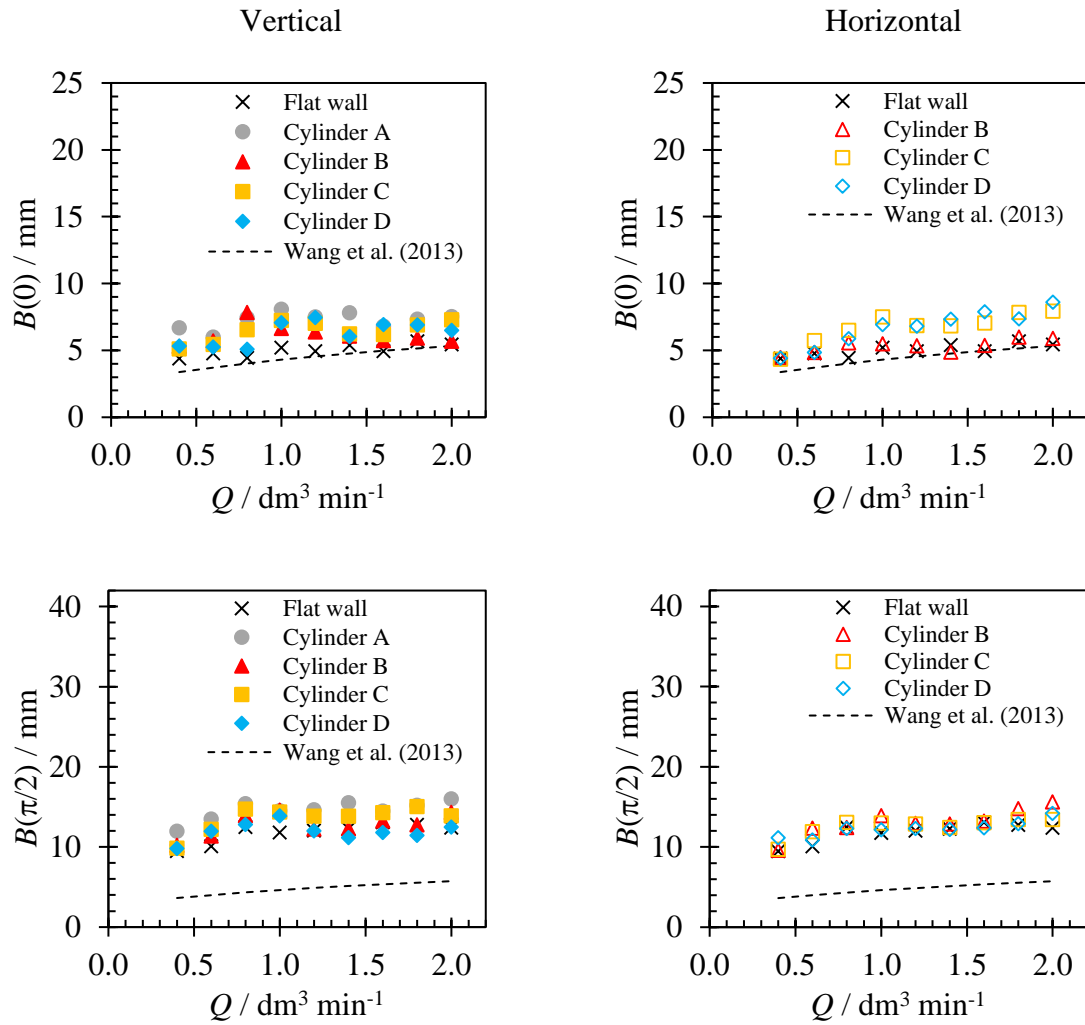


Figure S4 Effect of wall curvature on the width of the rope, $B(0)$, at the top of the RFZ and at the level of the impingement point, $B(\pi/2)$. Also plotted are the loci for the model for B presented by Wang *et al.* (2013). Conditions: coherent jets, $d_N = 2.0$ mm. Error bars omitted for clarity: these are approximately ± 2 mm for B and $\pm 0.1 \text{ dm}^3 \text{min}^{-1}$ for Q .